THE ASTROPHYSICAL JOURNAL, 294:242–255, 1985 July 1

SUBMILLIMETER OBSERVATIONS OF EVOLVED STARS

R. J. SOPKA[1]
University of Maryland and Catonsville Community College
R. HILDEBRAND[1]
Department of Astronomy and Astrophysics, Department of Physics, and Enrico Fermi Institute, University of Chicago
D. T. JAFFE[1,2]
Enrico Fermi Institute, University of Chicago
I. GATLEY
United Kingdom Infrared Telescope
T. ROELLIG AND M. WERNER
NASA/Ames Research Center
M. JURA
University of California at Los Angeles
B. ZUCKERMAN
University of Maryland and University of California at Los Angeles
Received 1984 May 29; accepted 1985 January 14

ABSTRACT

Broad-band submillimeter observations of the thermal emission from evolved stars have been obtained with the United Kingdom Infrared Telescope on Mauna Kea, Hawaii. These observations, at an effective wavelength of 400 μm, provide the most direct method for estimating the mass loss rate in dust from these stars and also help to define the long-wavelength thermal spectrum of the dust envelopes.

The mass loss rates in dust that we derive range from 10^{-9} to 10^{-6} $M_{\odot}$ yr^{-1} and are compared with mass loss rates derived from molecular line observations to estimate gas-to-dust ratios in outflowing envelopes. These values are found to be generally compatible with the interstellar gas-to-dust ratio of $\sim$100 if submillimeter emissivities appropriate to amorphous grain structures are assumed.

Our analysis of the spectrum of IRC +10216 confirms previous suggestions that the grain emissivity varies as $\lambda^{-1.2}$ rather than as λ^{-2} for $10 < \lambda < 1000$ μm. The overall properties of the model that we use in the analysis of IRC +10216 are found to be applicable to the similar carbon-rich object CRL 3068. Similar analysis of the spectra of oxygen-rich objects indicates that our submillimeter fluxes for IRC +10011 and NML Cyg are greater than those predicted by previous modeling. This, we argue, is the result of a slower decline in grain emissivity with wavelength than is seen in published silicate grain models.

We are not able to distinguish a systematic difference in the dust masses of carbon-rich and oxygen-rich envelopes. We find the largest mass loss rates in dust in the bipolar objects OH 231.8+4.2, CRL 2688, and CRL 618 and in NGC 7027 and VY CMa. The gas-to-dust mass ratios and the slopes of the far-infrared to submillimeter wavelength thermal continua that we derive are indicative of amorphous, rather than crystalline, grains in both carbon-rich and oxygen-rich envelopes.

Subject headings: infrared: sources — interstellar: grains — stars: circumstellar shells — stars: mass loss

I. INTRODUCTION

A wealth of observational evidence has shown that stellar evolution during the red giant stage is attended by a more or less steady process of mass loss. The gaseous component of the resulting circumstellar envelope is seen in the emission lines of a number of molecules which provide information on the kinematics of the outflowing material and the rate at which the star is losing mass. Observations at infrared wavelengths indicate the presence of dust grains coexisting with the gas in the envelope. A recent review of the properties of circumstellar envelopes is given by Zuckerman (1980).

Although the grains comprise a relatively small fraction of the mass of the circumstellar material, they may be largely responsible for driving the mass flow as a result of radiation pressure. In addition, the dust enters into the determination of the thermal state of the gas both as a result of collisional processes and to the extent that it shields the molecules from dissociation by the interstellar ultraviolet radiation field (Morris and Jura 1983*a*; Huggins and Glassgold 1982*a*, *b*).

Broad-band observations of thermal infrared emission from a large number of evolved stars at wavelengths $1 < \lambda < 20$ μm have clearly established the existence of dust grains (e.g., Merrill and Stein 1976*a*, *b*, *c*). Observations at higher spectral resolution are the basis for the generally held belief that the dust in the envelopes of M-type stars is composed of silicates, while in carbon-rich envelopes the grains are composed of some form of solid carbon (e.g., Merrill and Ridgway 1979).

Estimation of the total mass of dust from analysis of the intermediate infrared spectrum ($\lambda < 20$ μm) is complicated by

[1] Visiting Astronomer at the Infrared Telescope Facility, which is operated by the University of Hawaii under contract with the National Aeronautics and Space Administration.

[2] Now at the Space Sciences Laboratory, University of California, Berkeley.

two major model-dependent effects. Certainly in extreme cases, the dust is optically thick at these wavelengths, and, furthermore, the thermal emission per unit mass is very sensitive to the temperature of the grains. Observations at submillimeter wavelengths offer a method of overcoming these two problems. First, the dust is always optically thin when $\lambda > 100$ μm and consequently all parts of the envelope are sampled directly. Second, even at temperatures as low as 50 K, the submillimeter thermal emission falls on the Rayleigh-Jeans limit of the Planck function, thereby minimizing the uncertainty introduced by the grain temperature (e.g., Hildebrand 1983).

In this paper we describe observations of submillimeter thermal emission from a number of well-known evolved stars. Our program objects are chosen from among the brightest infrared sources and include stars with both carbon-rich and oxygen-rich envelopes. We compute estimates of the mass loss rate in dust for the envelopes based on our observed fluxes and, by comparison with existing CO emission-line data, derive estimates of the gas-to-dust mass ratio. The observations also provide additional information about the long-wavelength thermal spectrum of the circumstellar envelope which is determined by the mass distribution around the star and the wavelength dependence of the dust grain emissivity. We incorporate our observed 400 μm fluxes with observations of others at shorter wavelengths to model the far-infrared to submillimeter spectra of those objects for which we have detections.

II. OBSERVATIONS

Our data were obtained at the Mauna Kea Observatory in Hawaii primarily with the 3.8 m United Kingdom Infrared Telescope (UKIRT) during 1981 November 26–28. Additional data were obtained with the 3 m NASA Infrared Telescope (IRTF) in 1980 September. The submillimeter detectors used were the University of Chicago ^{4}He-cooled bolometer system (Whitcomb, Hildebrand, and Keene 1980) and the University of Chicago and NASA/Ames ^{3}He-cooled bolometer system of similar design.

An antimony-doped silicon bolometer, developed by H. Moseley (Goddard Space Flight Center) and M. Dragovan (University of Chicago) was used for the first time in this program. With this bolometer, the ^{4}He system had a noise equivalent flux density of $\sim$20 Jy Hz$^{-1/2}$. A bandpass of 300–800 μm was defined by interference filters at the short-wavelength limit (Whitcomb and Keene 1980) and diffraction and transmission of the field optics at the long-wavelength limit. The effective wavelength is determined by the instrumental response function, the atmospheric water-vapor content, and the shape of the source spectrum. In the UKIRT observations described herein, the effective wavelength was 400 μm and the FWHM beam size was 37″. For the IRTF observations, the effective wavelengths were 450 and 900 μm and the FWHM beam size was 47″. The ^{3}He system used on the UKIRT in 1981 November was similar in design to the ^{4}He system described above, but had 300–400 μm bandpass filtering.

Mars was used as the primary calibration standard, with fluxes derived from the brightness temperature model of Wright and Odenwald (1980). During the nights when the UKIRT observations were obtained, Mars was visible only during the early morning. Orion (OMC-1), W75N, and L1551 were used as secondary calibrators. Our determinations of their flux relative to Mars are presented in Table 1. Orion is extended, and so the flux in Table 1 represents only the portion of the source in the 37″ UKIRT beam.

TABLE 1

SECONDARY CALIBRATION[a] SOURCES

Object	Flux (Jy)	Temperature (K)
Orion	2025[b]	70
W75N	650	50
L1551	62	30

[a] Calibrated with respect to Mars, using data of Wright and Odenwald 1980.
[b] Within the UKIRT 37″ (FWHM) beam.

A beam-switching procedure was used to subtract the background flux produced by the sky and the telescope system. A chopping secondary mirror defined primary and reference beam positions 2.5–3.0 apart. We typically alternated integrations with the source placed in one beam for 10 s and then in the other for 10 s while chopping to the off-source position at 10 Hz. This procedure was generally repeated 10 times in sequence to obtain a set of integrations of 200 s total duration.

The results from both telescopes are presented in Table 2. The fluxes are shown with our estimate of the total error for all sets of integrations on a source and also a specification of the formal signal-to-noise ratio for each detection. The total errors reflect calibration uncertainties arising from variations in the mean for each set of integrations, uncertainties in the assumed spectral index and temperature for each source, uncertainty in the calibration of Mars (Wright 1976), and the signal-to-noise ratio in the data. The formal signal-to-noise ratio is presented separately to indicate the quality of the detections. Upper limits are 3 times the rms noise level in the final calibrated data.

In what follows, we attribute the 400 μm fluxes to thermal emission by the dust, although in the broad (300–800 μm) bandwidth there may be some contribution from molecular emission lines. For oxygen-rich envelopes, H_2O is a conceiv-

TABLE 2

OBSERVED SUBMILLIMETER FLUX[a]

	F_ν(400 μm)[b]		F_ν(450 μm)[d]		F_ν(900 μm)[d]	
OBJECT	(Jy)	S/N[c]	(Jy)	S/N[c]	(Jy)	S/N[c]
CRL 2688	41 ± 11	38	21 ± 8	5	...	...
IRC +10216	32 ± 8	20	29 ± 9	5	9 ± 3	5
OH 231.8+4.2	22 ± 5	11	<18	...	...	...
NGC 7027	19 ± 5	7	15 ± 6	3	...	...
VY CMa	10 ± 3	5	...	...	...	...
CRL 618	9 ± 3	8	<21	...	...	...
NML Cyg	7 ± 3	6	...	...	...	...
α Ori	4 ± 2	3	...	...	...	...
IRC +10011	3 ± 1	4	...	...	...	...
CRL 3068	2 ± 1	3	...	...	...	...
IRC +40540	<9	...	...	...	...	...
CIT 6	<7	...	<18	...	...	...
IRC −10529	<7	...	...	...	...	...
CRL 865	<6	...	...	...	...	...
o Ceti	<5	...	...	...	...	...
NML Tau	<4	...	...	...	...	...
IRC +60150	<4	...	...	...	...	...

[a] Corrected to outside Earth's atmosphere.
[b] UKIRT observation, 1981 November; 37″ (FWHM) beam.
[c] See § II.
[d] IRTF observation, 1980 September; 47″ (FWHM) beam.

able source of contaminating flux. The H_2O lines within our bandpass are due to transitions between high rotational levels (Poynter and Pickett 1981) and would not be expected to be significant unless maser action is occurring—a situation which is probably unlikely, but about which vitually nothing is known. SiO maser emission in M- and S-type stars is another conceivable source of contamination; these lines occur every $\sim$43 GHz and have been observed up to $J = 5$–4 (Clemens and Lane 1983). Observations of the unobscured SiO submillimeter transitions that fall in our band should be made.

The CO ($J = 6$–5) transition at 691 GHz (434 μm) has been detected in IRC +10216 (Koepf *et al.* 1982). By virtue of the relatively high abundance of CO, this transition is probably the strongest thermal emission line occurring in our bandwidth (although it is conceivable that the as yet unobserved CO ($J = 7$–6) transition may be stronger). The observed intensity of the CO ($J = 6$–5) transition of $T_A^* = 15$ K and line profile similar to that of the CO ($J = 1$–0) and CO ($J = 2$–1) lines would be equivalent to a flux of 0.4 Jy in a 300–800 μm band. This is sufficiently small to have no effect on the assumption that the observed flux is due to thermal emission by dust. HCN may contribute a comparable flux.

The total contribution from all possible molecular transitions in this frequency range is not known with any certainty (approximately 20 lines of $T_A^* = 10$ K and full width of 30 km s^{-1} would be required to produce a flux of 5 Jy), but the spectral scan of IRC +10216 obtained near 3 mm by Johansson *et al.* (1984) suggests that weak lines are insufficiently numerous to supply a significant flux. Weaker 400 μm sources in Table 2 also have weaker CO emission than IRC +10216 (e.g., Zuckerman 1978), so the ratio of line contamination to dust emission is not likely to vary greatly. Therefore, provided that maser emission can be discounted, it is not likely that molecular emission lines from already detected molecules contribute significantly to the fluxes we present. There is a variety of hydrides such as H_2S, SiH, and CH_2 whose lowest rotational transitions fall in our bandpass. Probably none of these lines contributes a significant portion of our measured flux, but they should be checked.

III. MASS LOSS RATES IN DUST

In principle, submillimeter observations provide the most direct means for estimating the total mass of circumstellar or interstellar dust in a given region. At these wavelengths even the most massive clouds are optically thin, and for $T \gtrsim 50$ K the Rayleigh-Jeans condition applies, thereby making the analysis relatively insensitive to the assumed dust temperature.

The gas in the envelopes of evolved stars is flowing radially outward at speeds that are known to good precision from the observed widths of molecular emission lines. Since it is reasonable to assume that the dust and gas move at nearly the same velocity (see below), it is convenient to estimate mass loss rates in dust rather than total dust masses, particularly since the extent of the dust envelope is not well known. (We describe in Appendix C a method for estimating the size of circumstellar envelopes.)

The observed flux at wavelength λ, from an element of volume dV, containing a number density of grains $n(r)$, with emission efficiency $Q(\lambda)$, and grain radius a, can be expressed as

$$dF_\nu(\lambda) = \frac{\pi a^2 Q(\lambda)}{d^2} B_\nu(\lambda, T(r)) n(r) P(r, \theta) dV \, . \tag{1}$$

Here $B_\nu(\lambda, T(r))$ is the blackbody intensity function whose value depends on the temperature at the radial distance r from the central star, d is the distance to the source, and $P(r, \theta)$ is the efficiency of the power pattern of the telescope beam, such that $P(r, \theta) \leq 1$, with θ measured relative to the star-Earth axis.

If the dust flows uniformly outward at velocity v_D, the mass loss rate in dust can be expressed as

$$\dot{M}_d = \tfrac{16}{3}\pi^2 a^3 \rho v_D r^2 n(r) \, , \tag{2}$$

where ρ is the average density of an individual grain.

Combining equations (1) and (2) with the usual expression for a volume element in spherical coordinates and assuming that $n(r) \propto r^{-2}$ (i.e., $\dot{M}_d = 0$), one finds, upon integrating,

$$F_\nu(\lambda) = \frac{\dot{M}_d}{v_D} \frac{\kappa_\nu(\lambda)}{2} \frac{\xi}{d^2} \, , \tag{3}$$

where

$$\xi = \iint B_\nu(\lambda, T(r)) P(r, \theta) \sin\theta \, d\theta \, dr \tag{4}$$

and

$$\kappa_\nu(\lambda) = \frac{3Q(\lambda)}{4a\rho} \, . \tag{5}$$

The relationship between the observed flux $F_\nu(\lambda)$ and the dust mass loss rate $\dot{M}_d$ thus requires a knowledge of the expansion velocity v_D, the integral expression ξ, the distance to the source d, and the cross section per unit mass of grain material $\kappa_\nu(\lambda)$. We now discuss each of these quantities.

a) Expansion Velocity v_D

The determination of the outflow velocity (v_D) of radiation pressure driven grains which are responsible for the observed expansion (v_g) of the gaseous envelope has been discussed by a number of authors (e.g., Gilman 1972; Goldreich and Scoville 1976; Kwan and Linke 1982). They have shown that the velocity of the dust relative to the gas (the drift velocity $v_{\rm drift}$) can be expressed as

$$v_{\rm drift} = \left(\frac{L v_g \bar{Q}_r}{\dot{M}_g c} \right)^{1/2} \, , \tag{6}$$

where L is the luminosity of the source, $\dot{M}_g$ is the mass loss rate in gas, c is the speed of light, and $\bar{Q}_r$ is the radiation pressure efficiency of the dust grains to emergent radiation. The dust velocity required in equation (3) is the sum of this drift velocity and the gas velocity. Note that if $\dot{M}_g v_g = L/c$, then $v_{\rm drift} = v_g \bar{Q}_r^{1/2}$.

For the average radiation pressure efficiency we adopt a value of 0.05 which is roughly twice that of Kwan and Linke (1982) but is comparable to that derived for the run of grain emissivities we find appropriate to model the spectra of both oxygen-rich and carbon-rich objects (see § V). $\dot{M}_g$ and v_g are taken from the various references we discuss in § IV. Table 3 shows our computed values of v_D and other quantities used in equation 6. In most cases, the drift velocity is small ($\lesssim$ a few km s^{-1}), and its inclusion typically alters the derived values of $\dot{M}_d$ by $\lesssim$20%.

b) Integral Expression ξ

The quantity ξ may be thought of as the convolution of the spatially distributed source function $B_\nu(\lambda, T)$ with the telescope beam pattern $P(r, \theta)$. The integration is carried out in a coordi-

TABLE 3

MASS LOSS RATES IN DUST AND GAS-TO-DUST RATIOS DERIVED FROM SUBMILLIMETER OBSERVATIONS

Object (1)	Observed $F_\nu(400\ \mu m)$ (Jy) (2)	Circumstellar $F_\nu(400\ \mu m)$ (Jy) (3)	d (pc) (4)	$\dot{M}_g$ ($M_\odot$ yr^{-1}) (5)	v_g (km s^{-1}) (6)	$\int F_\nu dv$ (W m^{-2}) (7)	L ($L_\odot$) (8)	v_D (km s^{-1}) (9)	$T(1'')$ (K) (10)	ζ[a] (11)	$\kappa_\nu(400\ \mu m)\dot{M}_d$ (cm^2 g^{-1})($M_\odot$ yr^{-1}) (12)	$\dot{M}_d$[b] ($M_\odot$ yr^{-1}) (13)	$\dot{M}_g/\dot{M}_d$[b] (14)	Notes
OH 231.8+4.2	22 ± 5	22	1300	1.0(−4)	70	7.4(−11)	3.9(+3)	72	85	3.7	1.4(−4)	7.1(−6)	14	1, 2
CRL 2688	41 ± 11	41	1000	7.2(−5)	19	7.9(−10)	2.5(+4)	22	116	3.9	4.6(−5)	2.3(−6)	31	3
NGC 7027	19 ± 5	15	1090	7.8(−5)	22	1.6(−10)	5.8(+3)	23	88	3.2	2.6(−5)	1.3(−6)	61	3
CRL 618	9 ± 3	9	1700	1.0(−4)	18	3.1(−10)	2.8(+4)	20	107	6.1	1.7(−5)	8.5(−7)	120	3
VY CMa	10 ± 3	10	1500	2.3(−4)	39	5.0(−9)	3.5(+5)	47	270	14	1.6(−5)	7.8(−7)	300	4
IRC +10216	32 ± 8	27	290	5.7(−5)	17	2.1(−8)	5.5(+4)	21	292	2.8	3.4(−6)	1.7(−7)	330	3
IRC +10011	3 ± 1	3	510	1.4(−5)	24	7.7(−10)	6.3(+3)	27	169	2.9	1.5(−6)	7.3(−8)	192	1
NML Cyg	7 ± 3	7	2000	>6.4(−5)	23	3.7(−9)	4.6(+5)	36	220	15	<1.3(−5)	<6.7(−7)	>95	5
			200	1.8(−6)	23	3.7(−9)	4.6(+3)	31	220	1.5	1.2(−6)	5.8(−8)	31	6
CRL 3068	2 ± 1	2	1000	2.0(−5)	14	3.2(−10)	1.0(+4)	17	110	3.7	1.8(−6)	8.9(−8)	224	1, 7
CRL 865	<6	<5	1580	1.5(−4)	14	1.5(−10)	1.2(+4)	15	111	5.9	<6.3(−6)	<3.2(−7)	>470	6
IRC +40540	<9	<7	960	8.0(−5)	15	5.9(−10)	1.7(+4)	17	167	5.4	<4.1(−6)	<2.0(−7)	>390	6
IRC −10529	<7	<7	620	1.0(−5)	17	6.1(−10)	7.3(+3)	21	155	3.2	<3.5(−6)	<1.8(−7)	>56	8
NML Tau	<4	<4	270	4.2(−6)	28	4.0(−9)	9.0(+3)	36	260	2.4	<8.8(−7)	<4.4(−8)	>96	6
IRC +60150	<4	<4	360	3.7(−6)	18	2.1(−9)	8.5(+3)	24	251	3.0	<8.5(−7)	<4.2(−8)	>88	6
CIT 6	<7	<6	190	3.7(−6)	17	2.1(−9)	2.3(+3)	20	203	1.3	<6.7(−7)	<3.3(−8)	>110	6
α Ori	4 ± 2	<4	200	4.0(−6)	15	8.5(−8)	1.1(+5)	35	574	3.9	<2.9(−7)	<1.4(−8)	>280	9
o Ceti	<5	<4	77	2.0(−7)	4	<2.4(−8)	<4.4(+3)	<13	>336	>0.9	<7.1(−8)	<3.5(−9)	>56	6

NOTE.—Numbers in parentheses: $1.0(-4) = 1.0 \times 10^{-4}$.

[a] Units for values shown, chosen to be compatible with customary units for other quantities in eq. (3), are 10^{13}(Jy pc^2)(km s^{-1})/($M_\odot$ yr^{-1})(cm^2 g^{-1}).

[b] Assuming $\kappa_\nu(400\ \mu m) = 20$ cm^2 g^{-1} (see text).

SOURCES OF DATA.—(1) $\dot{M}_g$, v_g from G. R. Knapp and M. Morris 1984, private communication; (2) distance from Bowers and Morris 1984; (3) $\dot{M}_g$ from Jura 1983*b*; (4) $\dot{M}_g$ from Bowers, Johnston, and Spencer 1983; (5) $d = 2$ kpc and $\dot{M}_g$ from Morris and Jura 1983*b*; (6) $\dot{M}_g$ from Knapp *et al.* 1982; (7) distance assuming $L = 10^4\ L_\odot$ and our total observed flux determination; (8) M_g from CO data of Zuckerman 1981 using Knapp *et al.* 1982 model; (9) $\dot{M}_g$ from Mauron *et al.* 1984.

nate system centered on the star with polar axis in the line-of-sight direction. The angle θ is then the polar angle of the volume element dV.

When computing ξ we make the following simplifications. First, the circumstellar envelope is spherical and has a density $n \propto r^{-2}$. Second, the telescope beam is a boxcar function, i.e., if $(2b/d)$ is the FWHM, then $P(r, \theta) = 1$ for $r \leq b$ and $P(r, \theta) = 0$ for $r > b$. Additionally, only the spherical volume within b is considered, and the source fills the beam. Third, the Rayleigh-Jeans approximation is used for $B_\nu(\lambda, T)$. Fourth, the entire shell is assumed to be optically thin to photospheric radiation, in which case $T(r) \propto r^{-\beta}$, where $\beta = 2/(4 + p)$ and p is the emissivity index defined by $Q \propto \lambda^{-p}$.

These assumptions allow a straightforward analytical evaluation of the ξ integral. In Appendix A we discuss a more complete treatment of this quantity and show that the values of ξ derived here are not severely affected by these assumptions.

With our assumptions, equation 4 becomes

$$\xi = \frac{4kT_0}{\lambda^2} r_0 \frac{(b/r_0)^{1-\beta}}{1-\beta}, \tag{7}$$

where T_0 and r_0 normalize the temperature profile so that $T = T_0(r/r_0)^{-\beta}$. We discuss in Appendix B a method for determining the dust temperature at an angular radius ϕ on the sky in the envelope where the nebula becomes optically thin to outflowing radiation. Since, in our objects, this occurs for angular distances $<1''$, it is convenient to take $r_0/d = 1''$ and normalize the temperature to $T_0 = T(1'')$ as computed by the method in Appendix B.

In terms of the customary units for the quantities in equation (3), we may write

$$\xi = 5.5 \times 10^{12} \frac{T(1'')d}{\lambda^2} \frac{(\phi_b/2)^{1-\beta}}{1-\beta}, \tag{8}$$

where the source distance d is in parsecs, $T(1'')$ is in K, λ is μm, ϕ_b is the FWHM beam diameter in arcsec as seen from Earth, and ξ is in units of (Jy pc^2)(km s^{-1})/($M_\odot$ yr^{-1})(cm^2 g^{-1}).

We use $p = 1.2$ (requiring $\beta = 0.38$) for both carbon- and oxygen-rich stars. This value is suggested by recent analyses of the envelopes of carbon stars (Jura 1983*a*; Rowan-Robinson and Harris 1983*b*), and, as we discuss in § V, provides the best fit to the far-infrared to millimeter spectrum of IRC +10216 and related objects. The long-wavelength spectra of the oxygen-rich envelopes we have modeled can also be approximated to good accuracy by taking $p = 1.2$.

c) *Distance d to the Source*

Since the integration to compute ξ is carried out in the frame of reference of the star, the fraction of the envelope seen by a telescope of fixed beamwidth increases with d. Consequently the computed value of ξ is directly dependent on the assumed value of d. Therefore, the functional relationship between F_ν and $\dot{M}_d$ is actually $F_\nu \propto d^{-1}\dot{M}_d$.

We have taken distances from the literature (cf. Cohen 1979; Hyland *et al.* 1972) but estimate that they are uncertain to no less than a factor of 2, and possibly in some cases as great as 10.

d) *Cross Section per Unit Mass of Grain Material, $\kappa_\nu(\lambda)$*

Although it is generally believed that the grains in the envelopes of oxygen-rich stars are composed of some form of silicate material, and that in carbon-rich environments carbon is the dominant grain constituent, the actual composition in both cases is unknown. Draine (1981) has recently surveyed the theoretical, experimental, and observational data relevant to the dust in the interstellar medium and presents a tabulation of absorption efficiencies for the carbon and silicate-based components. His conclusion that amorphous carbon is preferred to crystalline graphite is supported by the work of Jura (1983*a*) and Rowan-Robinson and Harris (1983*b*).

For silicate grains Draine (1981) has somewhat modified the absorption efficiencies of Jones and Merrill (1976) to comply with more recent observational constraints. Rowan-Robinson and Harris (1983*a*) show that such "dirty" silicate crystalline grains are adequate to model the $0.5 < \lambda < 50$ μm spectrum of oxygen-rich envelopes. We describe, however (in § V), a submillimeter excess seen in our observations for two such objects (IRC +10011 and NML Cyg) over that predicted on the basis of these crystalline silicate properties. We believe this to be the result of a significantly higher value of $\kappa_\nu(400\ \mu\text{m})$ than expected for crystalline silicates.

In this analysis, then, we adopt a value of $\kappa_\nu(400\ \mu\text{m}) = 20$ cm^2 g^{-1} for both the carbon-rich and the oxygen-rich stars. This is the value Draine (1981) derives for interstellar amorphous carbon, and it is thought to be a reasonable estimate for amorphous silicates. It is conceivable that this number could be different by an order of magnitude in either direction (we are considering circumstellar rather than interstellar grains) and not at all equal for the two grain materials. We will argue below, however, that the results of our analysis and those of others (Hildebrand 1983; Whitcomb *et al.* 1981) provide a reasonable basis for restricting this apparently wide range of uncertainty so that this adopted value for the mass opacity is probably good to within a factor of 3.

Table 3 shows the results of our analysis of the mass loss rates in dust derived from equation (3) along with other quantities required by the equations developed here. The program objects are listed in column (1) by their customary designations. Column (2) is our observed flux at 400 μm. Column (3) is our estimate of the portion of the observed flux originating from the nebula, derived by subtracting the photospheric contribution (NGC 7027 is corrected for free-free emission). Column (4) is the assumed source distance d. The mass loss rate in gas and the expansion velocity of the gas taken from various references are shown in columns (5) and (6). Our determination of the total observed flux and the resulting source luminosity are shown in columns (7) and (8). In column (9), the computed outflow velocity of the dust is shown. Column (10) is the dust temperature at an apparent angular radius of $1''$ used to normalize the temperature distribution through the envelope and computed by the method described in Appendix B. The analytical result for the integral ξ is shown in column (11). Because the uncertainty in the mass opacity of the dust is large, we show in column (12) $\kappa_\nu(400\ \mu\text{m})\dot{M}_d$. Column (13) is the mass loss rate in dust that we derive by assuming $\kappa_\nu(400\ \mu\text{m}) = 20$ cm^2 g^{-1} for all objects.

In view of the uncertainties in d and $\kappa_\nu(400\ \mu\text{m})$ already noted, the total uncertainty in the mass loss rates in dust (col. [13] of Table 3) is large. It is apparent, however, that the bipolar objects OH 231.8+4.2, CRL 2688, and CRL 618, the planetary nebula NGC 7027, and VY CMa have the largest mass loss rates in dust. Unless there is a significant difference in the mass opacity $\kappa_\nu(400\ \mu\text{m})$ of carbon and silicate grains, there is no obvious distinction between the mass loss rates in dust from carbon-rich and oxygen-rich stars that we observe.

IV. GAS-TO-DUST RATIOS

Mass loss rates in gas have been derived by others for a large number of evolved stars from analysis of molecular emission lines. Comparison of these values with our mass loss rates in dust yields estimates of the mass ratio of gas to dust in the outflowing material.

Knapp *et al.* (1982) have derived mass loss rates for most of our program objects from observations of CO—the strongest of the molecular emission lines seen in circumstellar envelopes. Jura (1983*b*) has evaluated the effects of dust shielding and molecular self-shielding on the spatial extent of CO envelopes, and derives mass loss rates that are generally smaller ($\sim 30\%$) than those of Knapp *et al.* and in better agreement with the detailed models of Kwan and Linke (1982) and Morris (1980). We therefore use the values for $\dot{M}_g$ derived by Jura for those objects to which he has applied his model (CRL 2688, NGC 7027, CRL 618, IRC +10216, IRC +10011, and CIT 6). For the other objects we take $\dot{M}_g$ from Knapp *et al.* (except when noted), although they may be as much as a factor of 5 too large.

Because of differences in the methods for determining $\dot{M}_g$ from molecular line observations, the relationship between $\dot{M}_g/\dot{M}_d$ and d depends on the reference from which $\dot{M}_g$ is taken. The analysis scheme presented by Knapp *et al.* (1982) results in $\dot{M}_g \propto d^2$, whereas Jura's (1983*b*) somewhat different approach implies $\dot{M}_g \propto d^{3/2}$. Our mass loss rates in dust have $\dot{M}_d \propto d$. Consequently, for the sources studied by Jura, $\dot{M}_g/\dot{M}_d \propto d^{1/2}$, while for the remaining objects, $\dot{M}_g/\dot{M}_d$ scales linearly with distance. We see no evidence for systematic errors in our derived values of $\dot{M}_g/\dot{M}_d$ arising from uncertainties in the distance estimates. Column (14) of Table 3 shows our estimate of $\dot{M}_g/\dot{M}_d$ for our adopted value of $\kappa_\nu(400\ \mu\text{m}) = 20\ \text{cm}^2\ \text{g}^{-1}$.

In view of the uncertainty in $\kappa_\nu(400\ \mu\text{m})$, the results for most of these evolved stars are generally consistent with $\dot{M}_g/\dot{M}_d \sim 100$, the typical interstellar value and that found for OH/IR stars by Werner *et al.* (1980). However, OH 231.8+4.2, CRL 2688, and NGC 7027 may well have relatively large proportions of dust in their circumstellar envelopes.

Jura (1983*b*) has considered the effects of anisotropic flow on the mass loss rates inferred from CO observations and found that departures from the customarily assumed spherical symmetry are unimportant. This is reassuring, since, at least in the visible and infrared, the objects that we find to have the largest $\dot{M}_d$ values and the lowest gas-to-dust ratios are not spherical.

V. SUBMILLIMETER SPECTRA OF CIRCUMSTELLAR ENVELOPES

The slope of the far-infrared to millimeter wavelength thermal spectrum of a circumstellar shell is determined by the distribution of dust mass and temperature through the shell. These two parameters, however, are not always independent, in that, unless the shell is optically thin to stellar radiation, the dust temperature is a function of the mass distribution and the wavelength variation of the grain emissivity.

Rowan-Robinson and Harris (1983*a*, *b*) have constructed consistent models for the infrared spectra of most of the reddest evolved stars in the AFGL survey (Price and Walker 1976) by assuming an $n(r) \propto r^{-2}$ grain number density variation and amorphous carbon-type grains for carbon-rich envelopes, and dirty silicate grains (Jones and Merrill 1976) for oxygen-rich envelopes. With the exception of IRC +10216, these models are compared with observed fluxes at $\lambda < 50\ \mu$m. Our observations at 400 μm extend the observed spectrum for a number of these objects. In this section we incorporate our data with existing observations and extend the model analysis to submillimeter wavelengths.

We have produced a detailed model of the radiation transfer through circumstellar dust shells that uses methods described by Leung (1975, 1976) and Rowan-Robinson (1980) to compute the temperature of the dust explicitly and predict the thermal spectrum of a spherically distributed circumstellar dust shell. Our emphasis is on the far-infrared to millimeter wavelength portion of the spectrum as constrained by our submillimeter observations.

Although our modeling procedure is essentially the same as that used by Rowan-Robinson and Harris (1983*a*, *b*), the sensitivity of submillimeter observations to the cooler component of the dust shell found at greater distance from the central star necessitates some additional considerations not included in their analysis. Care must be taken to extend the model dust shell to distances where the temperature drops to ~ 10 K (the Planck function peak for $\lambda = 400\ \mu$m). This, in turn, requires that attention be given to telescope beam-size effects in interpreting the observations, since, for most cases, the envelope is resolved at these wavelengths.

a) IRC +10216 and CRL 3068

IRC +10216 is the most extensively studied member of the class of evolved infrared stars. Broad-band observations over the range $1 < \lambda < 3300\ \mu$m have been obtained by a number of investigators, and, consequently, a reasonably complete spectrum can be presented. CRL 3068 is observationally similar to IRC +10216 in many respects (e.g., Merrill and Stein 1976*c*), but with an optically thicker dust envelope (Lebofsky and Rieke 1977; Jones *et al.* 1978).

To model IRC +10216, we follow Sutton *et al.* (1979), taking the central star to be an 1800 K blackbody of radius 0.″04, which corresponds to 2500 $R_\odot$ at a distance of 290 pc (Herbig and Zappala 1970). The inner and outer edges of the (assumed spherical) shell are set at 5 R_* (equivalent to 0.″2) and 30,000 R_* (20′). We have considered both the case of uniform outflow [$n(r) \propto r^{-2}$] and the density profile proposed by Fazio *et al.* (1980) in which $n(r) \propto r^{-1}$ for $r > 25''$. We concur with Rowan-Robinson and Harris (1983*b*) that, on the basis of model predictions, there is no compelling reason to depart from the uniform outflow condition. At the suggestion of Jura (1983*a*), we have used the optical constants for amorphous carbon tabulated by Draine (1981).

The results of our modeling of IRC +10216 are shown in Figure 1. The model fluxes at 50, 100, 200, and 1000 μm are derived by applying a telescope beam size (FWHM) of 84″ (Campbell *et al.* 1976) for the first three wavelengths and 55″ (Elias *et al.* 1978) for the last. For the 400 μm point the UKIRT 37″ beam size is used. Consequently the lines drawn in Figure 1 are only for illustrative purposes, since the beam sizes are not the same for all points. The upper curve shows the spectrum computed with the emissivities of Draine (1981), and the middle two solid curves result from a modification of these emissivities such that $Q \propto \lambda^{-p}$ for $\lambda > 10\ \mu$m. The best fit to the long-wavelength observations is found for $p = 1.2$. We attempted to fit the spectrum using the graphite grain parameters of Jones and Merrill (1976), but we find that a value of $p = 2$, as required by graphite, results in a model spectrum (*lower dashed curve*) that is much too steep to accommodate both the mid-infrared ($\lambda \sim 10\ \mu$m) and submillimeter-millimeter observations.

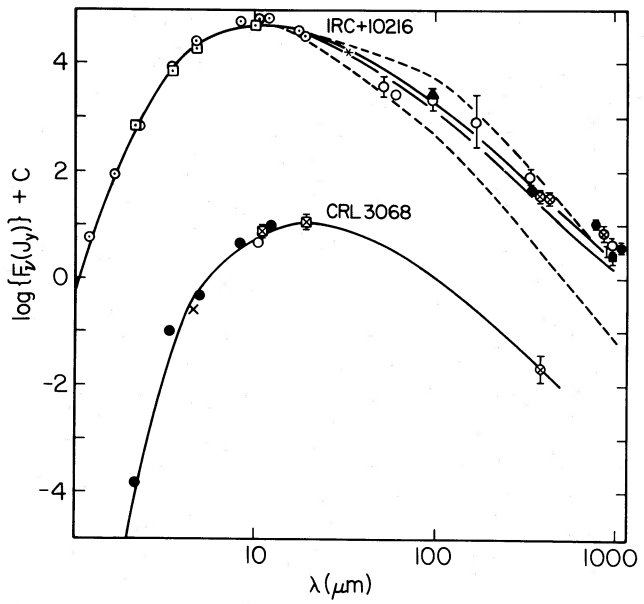

FIG. 1.—Model fits to the observed spectra of IRC +10216 and CRL 3068. In both cases, the model envelope is assumed to be spherically symmetric, with inner radius of 5 R_*, outer radius of 30,000 R_*, and to have a uniform outflow density distribution [$n(r) \propto r^{-2}$]. The central star is represented by an 1800 K blackbody of radius 2500 $R_\odot$. For IRC +10216, the upper dashed curve results from the amorphous carbon emissivities of Draine (1981). The lower dashed curve shows the long-wavelength trend dictated by the graphite grains of Jones and Merrill (1976). The solid curves represent a modification of Draine's emissivities such that $Q \propto \lambda^{-1.2}$ (*upper curve*) and $Q \propto \lambda^{-1.4}$ (*lower curve*) at $\lambda > 10$ μm. The values for C (*on ordinate*) are 0 and +2 for IRC +10216 and CRL 3068, respectively. Observational data for IRC+10216: *squares enclosing dots:* Becklin *et al.* (1969); *circled dots:* Strecker and Ney (1974); *asterisk:* Low, Rieke, and Armstrong (1973); *open circles:* Fazio *et al.* (1980); *filled triangle:* Shivanandan *et al.* (1977); *filled circles:* Phillips *et al.* (1982); *filled square:* Elias *et al.* (1978); *circled crosses:* present work. For CRL 3068, the solid curve represents the same model as described for IRC +10216, where $Q \propto \lambda^{-1.2}$, but with the optical depth in dust increased by a factor of 5. Observational data for CRL 3068: *filled circles:* Lebofsky and Rieke (1977); *open circle:* Lebofsky *et al.* (1976); *cross:* Joyce *et al.* (1977); *squares enclosing crosses:* Price and Walker (1976); *circled cross:* present work.

Mitchell and Robinson (1980) have shown that graphite particles in a model envelope provide a good fit to the observed 1–20 μm spectrum of IRC +10216 if the density variation is taken as $n(r) \propto r^{-1.3}$. Even when such a strong departure from the uniform outflow condition is assumed, their model indicates that the observed far-infrared to millimeter wavelength spectrum declines more slowly than predicted by graphite emissivities. Campbell *et al.* (1976) originally suggested that the slope of the observed long-wavelength thermal spectrum of IRC +10216 is indicative of grain emissivities larger than those of graphite.

The IRC +10216 models illustrated in Figure 1 correspond to the model for maximum light of Rowan-Robinson and Harris (1983*b*), although we require a 10 μm optical depth of 1.0, whereas they find $\tau(10\ \mu m) = 0.63$. The principal result of our analysis is to show that $p = 1.2$ is preferred on the basis of far-infrared to submillimeter wavelength observations. Rowan-Robinson and Harris do note that their best-fit model is probably not sufficiently extended to comply with the observed size of the molecular envelope, and a more extended model envelope would require an increase in p over their adopted value of $p = 1.0$.

The model we described for IRC +10216 is found to be easily applied to CRL 3068 if the optical depth in the dust shell is increased by a factor of 5. Although this object has not been observed at long wavelengths to the extent that IRC +10216 has been, our conclusion about the grain emissivity index is consistent with our 3 σ detection at 400 μm as shown in Figure 1. This analysis substantiates the conclusion of Jura (1983*a*) that the dust in the vicinity of IRC +10216 (and related objects) is characterized by an emissivity variation that suggests amorphous carbon rather than graphite grains having p-values suggested by most authors.

b) OH 231.8+4.2, CRL 2688, CRL 618, and NGC 7027

The optical structure of these objects departs so markedly from spherical symmetry that we have not attempted detailed modeling with our radiation transfer routine. Instead, we compare our 400 μm fluxes to extrapolations of simple models suggested by others as fits to the shorter wavelength ($\lambda < 100$ μm) portion of the spectra.

NGC 7027, CRL 618, and CRL 2688 are all carbon-rich objects that may represent extreme cases of carbon star evolution. CRL 618 and CRL 2688 have been described as proto–planetary nebulae (Zuckerman *et al.* 1976; Zuckerman *et al.* 1978; Lo and Bechis 1976), while the occurrence of a carbon-rich progenitor to NGC 7027 has recently been confirmed by the detection of HCN, which is seen only in evolved star envelopes where C/O ≥ 1 (Olofsson *et al.* 1982). OH 231.8+4.2 (also called OH 0739−14) is an oxygen-rich bipolar object whose morphological similarity to CRL 2688 has been described by Cohen and Frogel (1977).

Figure 2 shows a comparison of the spectra of these objects, and a reasonable similarity among them is apparent. On the other hand, the spectra display a notable dissimilarity to IRC +10216 and CRL 3068 as seen in Figure 1. (OH 231.8+4.2 has a spectrum also distinct from the more typical oxygen-rich stars discussed in the following section.) The peak emission occurs at wavelengths longer than in CRL 3068, but the shorter wavelength portion of the spectrum has a slope much less than that seen in the carbon stars, and, particularly in the case of NGC 7027, the long-wavelength spectrum is flatter. These characteristics of the observed spectra are similar to those of a larger sample of planetary nebulae described by Moseley (1980). That the far-infrared spectra of CRL 618 and CRL 2688 resemble those of planetary nebulae has been pointed out by Kleinmann *et al.* (1978).

The curves plotted in Figure 2 are derived from fitting isothermal models of the form $\lambda^{-p}B_\nu(\lambda, T)$ to the $20 < \lambda < 100$ μm data. For NGC 7027, McCarthy, Forrest, and Houck (1978) and Moseley (1980) obtain the best fit for $p = 2$ and $T = 90$ K. The values for p and T for OH 231.8+4.2, CRL 618, and CRL 2688 are 1.0 and 85, 1.5 and 95, and 1.5 and 100, respectively, as determined by Kleinmann *et al.* (1978).

There is ample evidence for the presence of dust within the ionized region of NGC 7027 (e.g., Becklin, Neugebauer, and Wynn-Williams 1973; Telesco and Harper 1977; Bentley 1982), while estimates of the proportion of circumnebular dust are less secure in the absence of mapping at submillimeter wavelengths. Kwok (1980) has shown that it is possible to model the main properties of the thermal spectrum of NGC 7027 with such a two-component model. Alternatively, the flattening of the $1 < \lambda < 10$ μm portion of the spectra of the bipolar objects may be the result of a disk geometry that allows scattered stellar photons to penetrate the thinner parts of the envelope.

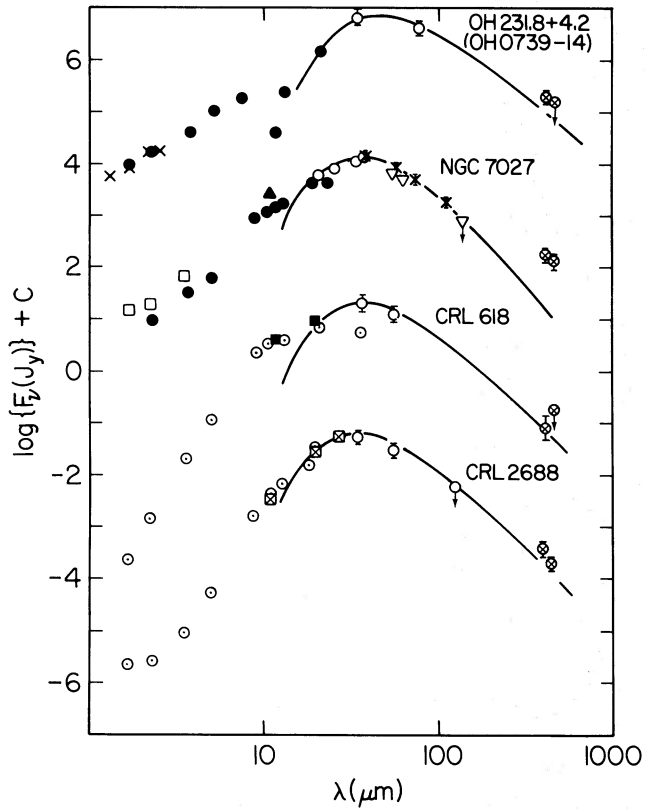

FIG. 2.—Model fits to the observed spectra of the bipolar objects, including the bipolar planetary nebula NGC 7027. Solid curves are of the general form $\lambda^{-p}B_\nu(\lambda, T)$. For OH 231.8+4.2, CRL 618, and CRL 2688, p and T are 1.0 and 85 K, 1.5 and 95 K, and 1.5 and 100 K, respectively, as determined by Kleinmann *et al.* (1978). For NGC 7027, $p = 2$ and $T = 90$ K as described by McCarthy, Forrest, and Houck (1978) and Moseley (1980). The values for C (*on ordinate*) are -4, -1, $+2$, and $+5$ for OH 231.8+4.2, NGC 7027, CRL 618, and CRL 2688, respectively. Observational data for OH 231.8+4.2: *crosses:* Sibille, Lunel, and Bergeat (1976); *filled circles:* Wynn-Williams, Becklin, and Neugebauer (1974); *open circles:* Kleinmann *et al.* (1978); *circled crosses:* present work. For NGC 7027: *open squares:* Willner, Becklin, and Visvanathan (1972); *filled circles:* Jameson *et al.* (1974); *open circles:* Dyck and Simon (1976); *crosses:* Moseley (1980); *inverted triangles:* Telesco and Harper (1977); *circled crosses:* present work. For CRL 618: *circled dots:* Westbrook *et al.* (1975); *filled squares:* Price and Walker (1976); *open circles:* Kleinmann *et al.* (1978); *circled crosses:* present work. For CRL 2688: *circled dots:* Ney *et al.* (1975); *squares enclosing crosses:* Price and Walker (1976); *open circles:* Kleinmann *et al.* (1978); *circled crosses:* present work.

We estimate that free-free emission from the ionized region of NGC 7027 contributes ~4 Jy to our observed flux of 19 Jy (Baars *et al.* 1977). The corrected value of 15 Jy is clearly inconsistent with the model of McCarthy, Forrest, and Houck (1978) and Moseley (1980), which predicts a value for the thermal flux of $F_\nu(400\ \mu\text{m}) \approx 2$ Jy. The excess thermal emission is probably due to the extended cooler circumnebular dust contained within the surrounding CO envelope observed by Mufson, Lyon, and Marionni (1975). Except for CRL 618, the other objects in Figure 2 also display a submillimeter excess over the models of Kleinmann *et al.* (1978).

c) *IRC +10011 and NML Cyg*

To incorporate our submillimeter observations with existing data, we have computed a series of models using IRC +10011 as a prototype. The observations of Zappala *et al.* (1974) and Hyland *et al.* (1972) are the basis for our chosen distance of 510 pc, stellar radius of 750 $R_\odot$, integrated flux of 8×10^{-10} W m^{-2}, and inner shell radius of 5 R_*. For reasons previously discussed, we extend the envelope to a distance where the dust temperature falls to $T \sim 10$ K and include the effect of resolution by the telescope beam to compute the flux at model points corresponding to far-infrared and submillimeter wavelengths.

The dirty silicate grain emissivities of Jones and Merrill (1976) are preferred by Rowan-Robinson and Harris (1983*a*). In our model of IRC +10011 that corresponds to their analysis of the maximum in the light cycle, the computed flux in the 20 μm resonance feature is too high. While we choose to suppress this in our computations by modifying the emissivities to produce a better fit to the observations, we will see that this has no significant effect on our conclusions about the submillimeter spectrum.

The results of our model calculation for IRC +10011 are shown in Figure 3. At 400 μm, we use a 37″ (FWHM) telescope beam, and, since there are no observations in the $30 < \lambda < 400$ μm range, we assign a beam size of 72″ to the 50, 100, and 200 μm points. (This represents the beam size of the *IRAS* telescope, which is the most likely source of observations near 50 and 100 μm.) The model spectrum resulting from the Jones and Merrill (1976) dirty silicate grain emissivities (modified near 20

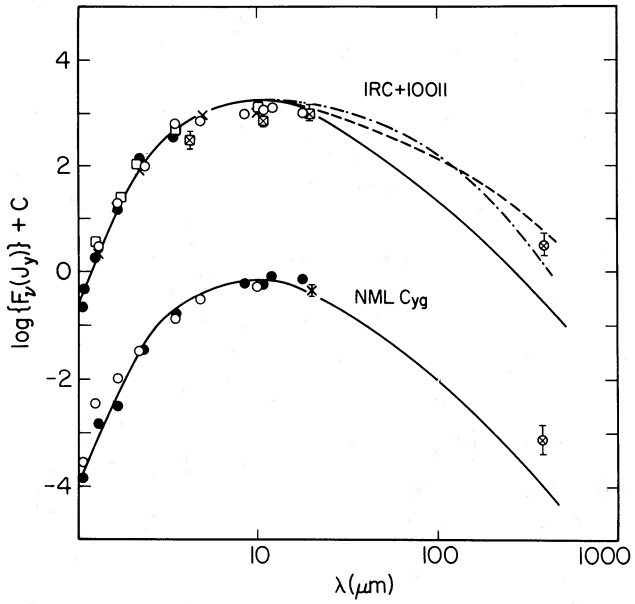

FIG. 3.—Model fits to the observed spectra of IRC +10011 and NML Cyg. The solid curves for both models are derived from a spherically symmetric, uniformly outflowing model shell using the grain emissivities of Draine (1981) and having $\tau(2.2\ \mu\text{m}) = 2.2$. The central star of IRC +10011 has a radius of 750 $R_\odot$ and $T_{\text{eff}} = 1950$ K. The dashed curve for IRC +10011 is computed assuming that $Q \propto \lambda^{-1}$ for $\lambda > 10$ μm, and the dash-dot curve for $n(r) \propto r^{-3/2}$ to account for the submillimeter excess (see text). For NML Cyg we use the same T_{eff} and adjust the stellar radius (and, therefore, the shell dimensions) to scale the model to the observed fluxes. The values for C (*on ordinate*) are 0 and +4 for IRC +10011 and NML Cyg, respectively. Observational data for IRC +10011: *filled circles:* Dyck, Lockwood, and Capps (1974); *crosses:* Zappala *et al.* (1974); *open circles:* Strecker and Ney (1974); *open squares:* Hyland *et al.* (1972); *squares enclosing crosses:* Price and Walker (1976); *circled cross:* present work. For NML Cyg: *open circles:* Hyland *et al.* (1972); *filled circles:* Strecker and Ney (1974); *cross:* Simon, Morrison, and Cruikshank (1972); *circled cross:* present work.

μm) predicts a flux at 400 μm approximately an order of magnitude less than we observe. When the same model spectrum is applied to NML Cyg (also shown in Fig. 3), we find a good fit in the $2 < \lambda < 20$ μm range, but again our observed flux significantly exceeds the model value.

There are two ways to enhance the submillimeter flux in the model computation: either the grain emissivity at submillimeter wavelengths can be increased, or the grain number density profile can be flattened to place a larger proportion of dust at a greater distance from the star (that is, at lower temperature). To examine the first of these alternatives, we compute a model for IRC +10011 with a grain emissivity that goes as $Q \propto \lambda^{-1}$ for $\lambda > 20$ μm, the result of which is plotted in Figure 3 and shows an acceptable fit to the observed spectrum including our 400 μm point. To illustrate how a flattening of the grain number density profile affects the model spectrum, we present (Fig. 3) a computation using $n(r) \propto r^{-3/2}$. For both IRC +10011 and NML Cyg, the lack of observational data at $20 < \lambda < 400$ μm makes it impossible to discount either of these alternatives on the basis of model fitting.

In the case of NML Cyg, it is conceivable that ambient cool interstellar dust could increase the observed 400 μm flux over that expected in a uniformly outflowing envelope. This object is close to the galactic plane and is affected by heavy interstellar obscuration, possibly as a result of its proximity to a nearby H II region (see Morris and Jura 1983*b* for a recent discussion). On the other hand, IRC +10011 is reasonably far from the galactic plane and shows no evidence for significant interstellar matter not originating from the central star. For this reason we think it unlikely that ambient cool dust is the cause of the observed submillimeter excess.

The choice between assigning the submillimeter excess to a relatively flat dust distribution [such that $n(r) \propto r^{-3/2}$] or to the radiative properties of the grains (such that $Q \propto \lambda^{-1}$) is difficult. We prefer the latter, since it has been suggested (e.g., Draine 1981) that an amorphous grain structure is a plausible way to account for enhanced long-wavelength emissivities. Forrest, McCarthy, and Houck (1979) argue that the lack of sharpness in the 10 and 20 μm emission features in the spectra of oxygen-rich envelopes is indicative of amorphous, disordered structures in the silicate grains. Furthermore, Morris and Jura (1983*b*) show that the radio continuum contours for NML Cyg agree well with a uniformly outflowing model for the gas.

Mezger, Mathis, and Panagia (1982) have computed absorption cross sections for amorphous silicates having a grain-size distribution that Mathis, Rumpl, and Nordsieck (1977) propose for the general interstellar medium, and find emissivities in the submillimeter range approximately 2 orders of magnitude greater than for crystalline silicates. Draine (1981) also makes the point that amorphous silicate structures are expected to have far-infrared emissivities at least an order of magnitude greater than for crystalline forms. While this is by no means a conclusive explanation for the submillimeter excess, it appears less arbitrary than postulating a significant departure from the uniform outflow model that would be required by the $n(r) \propto r^{-3/2}$ alternative.

This conclusion, that amorphous silicates may account for the observed submillimeter excess in the spectra of IRC +10011 and NML Cyg, is the basis for choosing $\kappa_\nu(400\ \mu\text{m}) = 20\ \text{cm}^2\ \text{g}^{-1}$ in deriving estimates of mass loss rates in dust in § III. This value results from our $Q \propto \lambda^{-1}$ modification of the emissivities of Jones and Merrill (1976) that fits the spectra as shown in Figure 3.

d) α Ori

Our observed flux of $F_\nu(400\ \mu\text{m}) = 4 \pm 2$ Jy for α Ori is consistent with that expected from photospheric emission, with possibly some contribution from the stellar chromosphere. A stellar diameter of 0".05 (Bonneau and Labeyrie 1973; Currie *et al.* 1976) and a photospheric temperature of $T_{\text{eff}} = 3250$ K (Dyck and Simon 1975) produce a blackbody flux of ~3 Jy, accounting for our detection and indicative of a very thin circumstellar shell around α Ori.

The radio spectrum of the chromospheric emission from α Ori from 1 to 10 GHz (Newell and Hjellming 1982) extrapolated to the submillimeter range predicts a flux of $F_\nu(400\ \mu\text{m}) \sim 1.5$ Jy, indicating that the crossover from the photospheric continuum to the chromospheric continuum occurs near 750 GHz.

VI. DISCUSSION

Our analysis of the far-infrared to submillimeter thermal spectra of the envelopes of carbon-rich and oxygen-rich stars indicates that, in both cases, the observed submillimeter flux exceeds that predicted by models using crystalline grains. In computing the gas-to-dust mass ratios presented in Table 3, we have used this result to justify assigning a value to the grain mass opacity of $\kappa_\nu(400\ \mu\text{m}) = 20\ \text{cm}^2\ \text{g}^{-1}$, which leads to values of $\dot{M}_g/\dot{M}_d$ generally compatible with the interstellar value of ~100.

The published emissivities for both graphite and crystalline silicate materials at 400 μm (Jones and Merrill 1976; Leung 1976; Draine 1981; Aannestad 1975; Mezger, Mathis, and Panagia 1982) result in values of $\kappa_\nu(400\ \mu\text{m})$ that are at least an order of magnitude less than our assumed value of $20\ \text{cm}^2\ \text{g}^{-1}$. Such low values would necessitate lowering by a factor of 10 the gas-to-dust ratios that we derive, thereby requiring that the material in some outflowing envelopes have a significantly greater proportion of dust than the general interstellar medium.

There is no way to account for a circumstellar gas-to-dust ratio as low as 1:10 without postulating either radically enhanced "heavy" element abundances or a grain composition that includes large amounts of hydrogen. The grains are much too hot to contain solid hydrogen, but, as least for the carbon-rich objects, greatly enhanced carbon abundances are conceivable, albeit unlikely. That is, if a large amount of carbon is produced by 3α reactions and mixed to the stellar surface, then [C]/[H] could be many times [O]/[H]. If all the excess carbon (i.e., [C] − [O]) is processed into grains, then $\dot{M}_g/\dot{M}_d$ could be substantially smaller than 100. It seems unlikely that this effect could be responsible for small ratios of $\dot{M}_g/\dot{M}_d$ in all carbon-rich objects (since, generally, the carbon-to-oxygen ratio is probably not much greater than unity), but it might occasionally be important.

Hildebrand (1983) has recently analyzed various observational aspects of cool interstellar dust clouds and estimates values for the grains parameter that best typify the dust associated with these objects. Dust found in the interstellar medium is likely to be more heterogeneous than that produced in outflowing stellar envelopes, so his values probably represent an "average" dust species whose properties are a composite of those of carbon and silicate grains. Possibly the grains are also coated with interstellar material and "processed" by the interstellar ultraviolet radiation field. Hildebrand suggests a value of $\kappa_\nu(400\ \mu\text{m}) \sim 6\ \text{cm}^2\ \text{g}^{-1}$, with an uncertainty of a factor of 3–4. Such a lower value for $\kappa_\nu(400\ \mu\text{m})$ would give uncom-

fortably low values for $\dot{M}_g/\dot{M}_d$ for a number of our objects. Consequently, we believe that our value of $\kappa_\nu(400\ \mu\text{m}) = 20\ \text{cm}^2\ \text{g}^{-1}$ is probably good to within a factor of 2–3. Thus, the analyses of the gas-to-dust ratios and the submillimeter thermal spectra we present here provide reasonably strong evidence that the mass opacity of the dust at submillimeter wavelengths cannot be accounted for by assuming the existence of crystalline materials.

For oxygen-rich envelopes displaying OH maser emission, it is possible to use our observations to estimate the ratio of the emissivities at ultraviolet and submillimeter wavelengths by analyzing the radial extent of OH maser emission. Huggins and Glassgold (1982*b*) show that H_2O in oxygen-rich environments is photodissociated when the dust optical depth to interstellar ultraviolet radiation drops sufficiently. The main product of the dissociation is OH, which is observed in maser emission in four of our program objects, OH 231.8+4.2, IRC +10011, NML Cyg, and VY CMa. The analysis of Huggins and Glassgold indicates that the location of the maser emission coincides with the radial distance where the OH number density peaks. Observations of the phase difference between the blue- and redshifted components of the 1667 MHz OH maser line yield the line-of-sight dimension of the emitting region (cf. Jewell, Webber, and Snyder 1980; Bowers, Johnston, and Spencer 1983) which may be used to fix the distance from the central star where H_2O dissociation occurs.

For a uniformly expanding shell, the optical depth in dust from a point r out to infinity can be expressed as

$$\tau(r \rightarrow \infty) = \frac{\kappa_\nu(\lambda)}{4\pi r} \frac{\dot{M}_d}{v_D} . \tag{9}$$

If we describe the relative dust opacity from ultraviolet (0.15 μm) to submillimeter (400 μm) wavelengths as

$$\kappa_\nu(\text{UV}) = \kappa_\nu(\text{sub-mm}) \left(\frac{\lambda_{\text{UV}}}{\lambda_{\text{sub-mm}}} \right)^{-p} , \tag{10}$$

the optical depth becomes

$$\tau_{\text{UV}}(r) = \frac{\kappa_\nu(400\ \mu\text{m})}{4\pi r} \frac{\dot{M}_d}{v_D} \left(\frac{400}{0.15} \right)^p . \tag{11}$$

Using equation (3), we substitute to obtain

$$\tau_{\text{UV}}(r) = \frac{d^2 F_\nu(400\ \mu\text{m})}{2\pi r \xi} \left(\frac{400}{0.15} \right)^p , \tag{12}$$

and, therefore,

$$p = 0.29 \log \left[\frac{2\pi r \tau_{\text{UV}}(r) \xi}{d^2 F_\nu(400\ \mu\text{m})} \right] . \tag{13}$$

We take r to be the radial distance at which H_2O is photodissociated to form OH as dictated by the dimensions of the maser region. At this point in the envelope it is reasonable to assume that $\tau_{\text{UV}}(r) \sim 2$, and we use our observed values of $F_\nu(400\ \mu\text{m})$ with appropriate choices for ξ and d to determine p.

Applying values of r of 3.3×10^{16}, 9×10^{16}, 4.8×10^{16}, and 8.1×10^{16} cm for IRC +10011, OH 231.8+4.2, VY CMa, and NML Cyg, respectively (Jewell, Webber, and Snyder 1980; Bowers, Johnston, and Spencer 1983; Bowers and Morris 1984), we find that our observed fluxes result in $p \sim 1.0$ for OH 231.8+4.2, $p \sim 1.1$ for VY CMa, $p \sim 1.2$ for IRC +10011, and $p \sim 1.3$ for NML Cyg (assuming $d = 2$ kpc).

Aannestad (1975), Jones and Merrill (1976), and Draine (1981) derive values of $p > 1.5$ for crystalline silicate grains, whereas Mezger, Mathis, and Panagia (1982) present values for amorphous silicates that result in $p = 0.9$. Again, the evidence points to disordered amorphous structures for the silicate grains in preference to crystalline structures.

Jura (1983*a*) has carried out a similar analysis for the carbon-rich envelope around IRC +10216. By analyzing the extent of HCN emission, which is determined by the radial distance at which dust shielding becomes incapable of protecting the HCN from photodissociation by interstellar UV photons, and comparing the resulting UV optical depth to that at 100 μm, Jura shows that the emissivity of carbon grains varies as $\lambda^{-1.3}$ over 5 orders of magnitude in wavelength.

VII. CONCLUSIONS

To summarize, the main conclusions that we find from the analysis of our 400 μm observations of evolved star envelopes are as follows:

1. The largest values of the mass loss rate in dust are found for the bipolar objects OH 231.8+4.2, CRL 2688, and CRL 618 and the bipolar planetary nebula NGC 7027. In addition, VY CMa, an object of uncertain ancestry, and NML Cyg, if it is 2 kpc distant (Morris and Jura 1983*b*), exhibit relatively large mass loss rates. The derived values for the mass loss rates in dust are limited in accuracy by the uncertainties in the assumed source distance and the opacity per gram at 400 μm.

2. The gas-to-dust mass ratios in evolved star envelopes are, in general, comparable to the interstellar value of 100 if the 400 μm opacity is $\kappa_\nu(400\ \mu\text{m}) = 20\ \text{cm}^2\ \text{g}^{-1}$. With the exception of VY CMa, the objects having the largest mass loss rates in dust show the smallest $\dot{M}_g/\dot{M}_d$ with OH 231.8+4.2 and CRL 2688 exhibiting the lowest values.

3. If the mass distribution in evolved star envelopes is adequately represented by the uniform outflow condition [$n(r) \propto r^{-2}$], then the far-infrared to submillimeter spectra of both the carbon-rich and the oxygen-rich objects are less steep than would be implied by the emissivities of crystalline grain materials. This result, when taken in conjunction with reasonable assumptions about lower limits to the gas-to-dust ratio, precludes submillimeter emissivities derived for crystalline materials, thus supporting the conclusion that amorphous structures in both carbon and silicate grains are found in outflowing envelopes.

We thank Dr. Herbert Pickett for kindly providing us with information on the submillimeter water vapor lines. We are also grateful to Dr. Jocelyn Keene for assistance with the calibration of the IRTF observations and to Drs. Ned Wright and Mark Morris for their helpful comments on an early version of this manuscript. We thank the University of Hawaii for granting us time on the UKIRT and gratefully acknowledge the support staffs of both the UKIRT and the IRTF observatories for their able assistance.

This research was partially supported by NSF grant AST 8023355 to the University of Maryland, NASA grant NAG-W-4 to the University of Chicago, and a NASA grant to UCLA. The computer time for this project was supported in part through the facilities of the Computer Science Center of the University of Maryland.

APPENDIX A

DETERMINATION OF THE INTEGRAL EXPRESSION ξ

We have previously described the integral expression ξ (defined in eq. [4]) as the convolution of the source function $B_\nu(\lambda, T)$ with the telescope beam pattern $P(r, \theta)$. For a given wavelength, $B_\nu(\lambda, T)$ is a single-valued function of temperature which depends on position in the circumstellar envelope. If the envelope is optically thin at λ, ξ is the integral of this function throughout the volume of the nebula weighted by $P(r, \theta)$. Figure 4 shows the geometry of the volume to be considered for the case of a spherical shell observed by a telescope of FWHM beam size $2b$, positioned on the central star. In effect, the telescope samples a cylindrical section along a diameter of the spherical shell.

To perform the volume integration, the temperature distribution and $P(r, \theta)$ must be functionally represented, and the inner and outer shell boundaries established to fix the integration limits.

The assumptions we impose in § III to derive the analytical expression for ξ may be relaxed, but at the expense of computational simplicity. Here we present the results of numerical calculations for the case of IRC +10216, using a Gaussian beam pattern and a temperature distribution explicitly computed by radiation transfer methods. The purpose of this exercise is to demonstrate quantitatively the relatively small error introduced by using the analytical form for ξ.

The upper panel of Figure 5 shows the temperature profile we compute for IRC +10216 for the best model fit to the observed spectrum (see § V). The corresponding optically thin approximation in which $T \propto r^{-2/(4+p)}$ is also indicated. The function $\xi(r)$, which, for a Gaussian beam, becomes

$$\xi(r) = \int_{r_i}^{r} B_\nu(\lambda, T)\left\{2\int_0^{\pi/2} \exp\left[-0.69\left(\frac{r\sin\theta}{b}\right)^2\right]\sin\theta d\theta\right\}dr\,, \tag{A1}$$

is shown in the lower panel of Figure 5. The solid lines show the value of the function for half-power beam radius, $b = 100\,R_*$, 460 R_*, 1000 R_*, and ∞. For IRC +10216 (with an inner shell boundary $r_i = 5\ R_* = 0''.2$) these correspond to FWHM Gaussian beamwidths of 8″, 37″, 80″, and ∞. By comparing $\xi(r = b)$ to the asymptotic value for each curve, one may determine the fraction of the total flux in the beam that arises from a spherical volume of radius b. We see that >75% of the observed flux is accounted for if the portion of the envelope within the cylindrical volume delimited by the half-power beam radius (see Fig. 4), but at $r > b$ from the central star, is ignored (as we have done in computing ξ in § III).

The dashed curve in the lower panel of Figure 5 indicates the discrepancy introduced by using the Rayleigh-Jeans approximation for $B_\nu(\lambda, T)$. Unless the telescope beam reaches to envelope regions where $hc/k\lambda T < 1$, only a small (<15%) overestimate of the flux results from assuming the Rayleigh-Jeans limit.

We have performed identical analyses where the beam pattern is a boxcar function and, also, where it is a parabola. The assumed beam shape has virtually no (<5%) effect of the results for $\xi(r)$.

Finally, we have replaced the model-generated temperature profile with the power-law form, $T \propto r^{-2/(4+p)}$. By doing this, we ignore the steepening of $T(r)$ in the optically thick, inner region of the envelope. For the circumstellar shells that we are investigating, this region contains a very small fraction of the mass of the envelope, and our calculations show the loss of flux to be <2% when it is ignored.

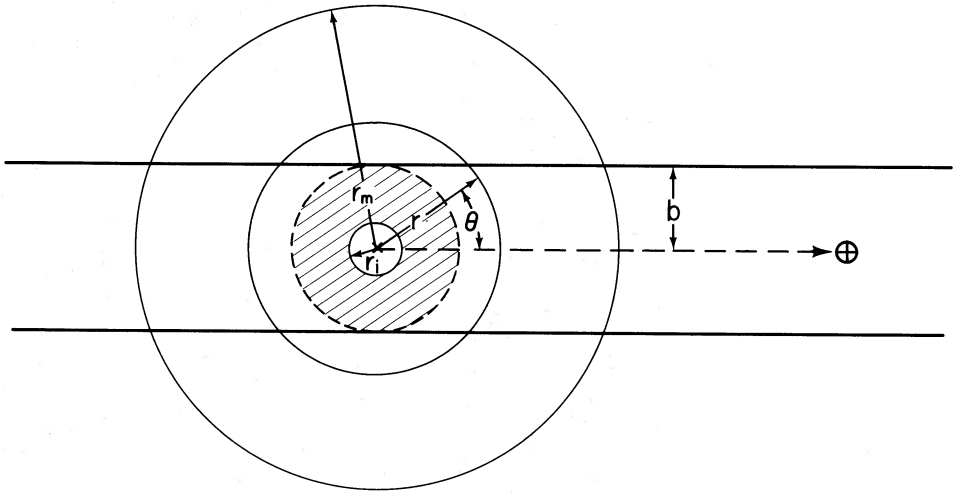

FIG. 4.—An illustration of the geometry required for the integral expression ξ. The radius of the inner edge of the spherical shell is r_i, and the linear diameter of the telescope beam at the source is $2b$. The outer radius, r_m, is set where the dust temperature drops to ~10 K. In the analytical form of ξ used in § III to compute mass loss rates, only the shaded region is included (and r_i is set to zero). The numerical procedure discussed in Appendix A includes the cylindrical section of radius b that extends through the spherical shell.

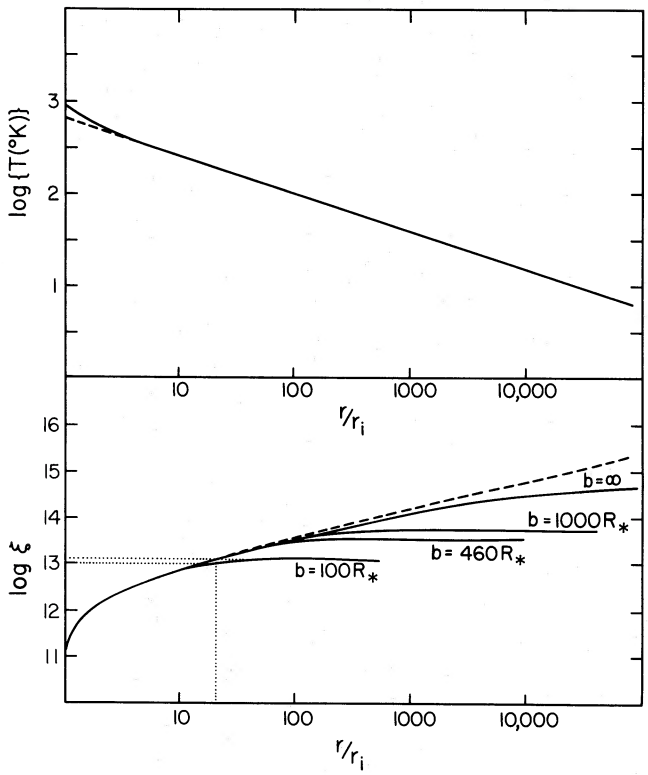

FIG. 5.—(*Upper panel*) The computed dust temperature through the model envelope of IRC +10216 is shown by the solid line (see § V for discussion of the model parameters). The dashed curve is the extrapolation of an optically thin temperature distribution which coincides with the model curve at large radii. A negligible fraction of the dust is affected by assuming that the temperature profile throughout is given by $T \propto r^{-\beta}$ as long as the envelope is not highly resolved. (*Lower panel*) Numerically computed values of the integral expression $\xi(r)$ (see Appendix A) are shown for various telescope beam sizes b. In these curves, the inner radius of the envelope is $r_i = 5\ R_*$. The fraction of the long-wavelength flux originating in the spherical volume of radius b (shown in Fig. 4) can be calculated by comparing $\xi(r = b)$ with the asymptotic limit for the curve. For example, the asymptotic value for the $b = 100\ R_* = 20\ r_i$ curve is shown by the upper horizontal dotted line. The lower dotted line shows the value of ξ corresponding to $r/r_i = 20$. The difference Δ (log $\xi \sim 0.1$) indicates that $\sim 13\%$ of the total flux that is intercepted by the telescope beam originates outside the spherical volume of radius b. The dashed curve results if the Rayleigh-Jeans expression is used for $B_\nu(\lambda, T)$. The units for ξ are chosen to be compatible with the customary units for the other quantities in eqn. (4) and are (Jy pc^2)(km s^{-1})/($M_\odot$yr^{-1})(cm^2 g^{-1}).

APPENDIX B

NORMALIZATION OF THE TEMPERATURE PROFILE

In the preceding section, we have noted that the temperature distribution through a circumstellar shell may be adequately represented by $T \propto r^{-2/(4+p)}$ when relating the observed submillimeter flux to the mass of dust. Here we describe a method for normalizing this temperature distribution.

To compute the steady state temperature of a dust grain, we set the energy absorbed equal to the energy that is emitted. These quantities depend upon the efficiency with which the grain absorbs (and emits) light and the mean intensity of the local radiation field. For a very dusty star, the spectral energy distribution in the inner portion of the envelope is a complicated function of position because optical light is converted into infrared. However, beyond the inner envelope, the spectrum is essentially fixed and all that changes is the geometric dilution. Therefore, the flux of a star observed at Earth can be used to find the radiation density in the outer circumstellar envelope, from which we can compute the temperature distribution.

If $Q(\nu)$ is the ratio of absorption to geometric cross section, so that $Q(\nu) = Q_0(\nu/\nu_0)^p$, we can calculate the temperature distribution as a function of ϕ, the observed angular displacement from the star for a point in the plane of the sky. In a steady state, the temperature T is given by

$$\int_0^\infty \frac{F_\nu(\nu)}{4\pi\phi^2} Q_0 \left(\frac{\nu}{\nu_0}\right)^p d\nu = \int_0^\infty Q_0 \left(\frac{\nu}{\nu_0}\right)^p B_\nu(\nu, T) d\nu \,, \tag{B1}$$

where the mean intensity at ϕ is $F_\nu/4\pi\phi^2$ and $F_\nu(\nu)$ is the observed flux at frequency ν. We define $f(p)$ as

$$f(p) = \int_0^\infty \frac{x^{3+p}}{e^x - 1}\, dx \,. \tag{B2}$$

To within 10%, $f(p) = (p + 3)!$ for $p \geq 0$.

The solution to equation (B1) for T as a function of ϕ is given by

$$T(\phi) = \phi^{-2/(4+p)} \frac{h}{k} \left[\frac{c^2}{8\pi h f(p)} \int_0^\infty \nu^p F_\nu(\nu) d\nu \right]^{1/(4+p)} . \tag{B3}$$

In the above expression, h, k, and c are Planck's constant, the Boltzmann constant, and the speed of light, respectively. Note that at say, 1″ from the star, T is relatively insensitive to p and very insensitive to the actual observed flux.

APPENDIX C

SIZE OF CIRCUMSTELLAR ENVELOPES

One of the major uncertainties regarding the outflows from late-type stars is the nature of the grains and their role in the dynamics. Here we discuss possible measurements of the far-infrared sizes of circumstellar envelopes, and we find that the diameter of the aperture in which half of the total power is observed, the half-power size, is a very sensitive probe of the far-infrared emissivity of the grains. It should be recognized that the half-power size of the source is very different from the FWHM measured with a Gaussian beam, the only type of size measurement that is currently available (see Fazio *et al.* 1980).

Consider, for example, a circumstellar envelope where $n(r)$ varies as r^{-2} and T varies as $r^{-0.4}$. In this case, when the Planck function can be approximated in the Rayleigh-Jeans limit, the surface brightness S varies as $\phi^{-1.4}$, where ϕ is the apparent angular radius of a point in the envelope as seen from the Earth. With such a power-law distribution of the surface brightness, the only scale size is set by the telescope beam, and it is straightforward to show that the observed FWHM of the circumstellar envelope is 1.2 times the FWHM of the telescope beam (Fazio *et al.* 1980; Rowan-Robinson and Harris 1983*b*). However, since S varies as $\phi^{-1.4}$ and an element of solid angle varies as $\phi d\phi$, the total flux from the circumstellar envelope can be very much larger than twice what is measured in the FWHM map of the object. That is, since most of the energy is emitted in the outer regions of very low surface brightness, a simple scan with a Gaussian beam to determine where the intensity falls to half its peak value may not be a good measure of the full extent of the emission.

The luminosity of a circumstellar envelope within a radius r_c can be written in the optically thin approximation as

$$L(r_c) = \int_0^{r_c} \chi_\nu(r) 4\pi B_\nu(\nu, T) 4\pi r^2 dr , \tag{C1}$$

where the volume opacity $\chi_\nu(r) = \pi a^2 Q(\nu) n(r)$. If we assume that the opacity varies so that $\chi_\nu = (\chi_\nu)_0 (r_0/r)^2$, then

$$L(r_c) = (4\pi)^2 (\chi_\nu)_0 r_0^2 \int_0^{r_c} B_\nu(\nu, T) dr . \tag{C2}$$

We denote $r_{1/2}$ as the radius at which half the energy is emitted; that is, we set $L(r_{1/2}) = L(\infty)/2$. As discussed previously, most of the energy emitted into a beam of projected radius b is from the sphere centered around the star with actual radius b, so if one is able to determine the beam size in which a power of $L(\infty)/2$ is received, then the size will correspond approximately to $r_{1/2}$. If we set $T = T_0 (r_0/r)^\beta$ and $x = (r/r_0)^\beta h\nu/kT_0$, we may rewrite equation (C2) as

$$L(x_c) = (4\pi)^2 (\chi_\nu)_0 r_0^3 \frac{2h\nu^3}{c^2 \beta} \left(\frac{kT_0}{h\nu} \right)^{1/\beta} \int_0^{x_c} \frac{x^{1/\beta - 1}}{e^x - 1} dx . \tag{C3}$$

It is straightforward to show numerically from equation (C3) that in the range of interest where $0.3 \leq \beta \leq 0.4$, $x_{1/2} = 1.15(1/\beta - 1)$. Incidentally, if we replace $(e^x - 1)$ with e^x, equation (C3) would be an incomplete gamma function, and a similar result would follow. In any case, we find that

$$r_{1/2} = r_0 (x_{1/2})^{1/\beta} \left(\frac{kT_0}{h\nu} \right)^{1/\beta} = r_0 \left[1.15 \left(\frac{1}{\beta} - 1 \right) \right]^{1/\beta} \left(\frac{kT_0}{h\nu} \right)^{1/\beta} . \tag{C4}$$

Equation (C4) shows that $r_{1/2}$ is a strong function of β, which in turn depends upon the emissivity of the grains. That is, if the emissivity varies as ν^{+1} or ν^{+2}, then $\beta = 0.4$ and 0.33, respectively. We then find from equation (C4) that $r_{1/2} = 4r_0 (kT_0/h\nu)^{2.5}$ and $r_{1/2} = 12 r_0 (kT_0/h\nu)^{3.0}$, respectively. This difference is very marked. Consider, for example, IRC +10216 at 100 μm. At $r_0 = 1''$, $T_0 = 285$ K and $T = 320$ K for $\beta = 0.4$ and 0.33, respectively, so that the half-power sizes are predicted to be 22″ and 131″, respectively.

It should be noted that the number density variation of the grains with radius can also strongly affect the half-power size. If, for example, $n(r)$ varies as $r^{-1.5}$ instead of r^{-2}, then equation (C4) is modified in a simple way to

$$r_{1/2} = r_0 \left[1.15 \left(\frac{1.5}{\beta} - 1 \right) \right]^{1/\beta} \left(\frac{kT_0}{h\nu} \right)^{1/\beta} . \tag{C5}$$

As a result, the half-power sizes of IRC +10216 at 100 μm are computed to be 98″ and 744″ for $\beta = 0.4$ and 0.33, respectively.

That there are very large differences among the half-power sizes is straightforward to understand. The surface brightness of the circumstellar envelope should appear as a power law with an exponential cutoff; most of the energy of the shell is emitted near the

cutoff. The grains with a stronger emissivity as a function of frequency display a flatter power-law surface brightness, with the result that proportionately more energy is emitted near the exponential cutoff, so the half-power size appears substantially larger. Similarly, if the density distribution of the grains is less steep, most of the power is emitted even farther from the central star. It should be noted, however, that at very long wavelengths (for example at 400 μm) these calculations do not apply because the interstellar radiation field will maintain the grains at a sufficiently high temperature that they will be effective radiators and there will be no outer exponential cutoff. Also, at wavelengths <20 μm, a power-law distribution of temperature is not appropriate because it is not likely that the grains survive at temperatures much in excess of 1000 K.

REFERENCES

Aannestad, P. A. 1975, *Ap. J.*, **200**, 30.
Baars, J. W., Genzel, R., Pauliny-Toth, I. I. K., and Witzel, A. 1977, *Astr. Ap.*, **61**, 99.
Becklin, E. E., Frogel, J. A., Hyland, A. R., Kristian, J., and Neugebauer, G. 1969, *Ap. J. (Letters)*, **158**, L133.
Becklin, E. E., Neugebauer, G., and Wynn-Williams, C. G. 1973, *Ap. Letters*, **15**, 87.
Bentley, A. F. 1982, *A.J.*, **87**, 1810.
Bonneau, D., and Labeyrie, A. 1973, *Ap. J. (Letters)*, **181**, L1.
Bowers, P. F., Johnston, K. J., and Spencer, J. H. 1983, *Ap. J.*, **274**, 733.
Bowers, P. F., and Morris, M. 1984, *Ap. J.*, **276**, 646.
Campbell, M. F., *et al.* 1976, *Ap. J.*, **208**, 396.
Clemens, D. P., and Lane, A. P. 1983, *Ap. J. (Letters)*, **266**, L117.
Cohen, J. G., and Frogel, J. A. 1977, *Ap. J.*, **211**, L78.
Cohen, M. 1979, *M.N.R.A.S.*, **186**, 837.
Currie, D. G., Knapp, S. L., Liewer, K. M., and Braunstein, R. H. 1976, University of Maryland Technical Report 76-126.
Draine, B. T. 1981, *Ap. J.*, **245**, 880.
Dyck, H. M., Lockwood, G. W., and Capps, R. W. 1974, *Ap. J.*, **189**, 89.
Dyck, H. M., and Simon, T. 1975, *Ap. J.*, **195**, 689.
———. 1976, *Pub. A.S.P.*, **88**, 838.
Elias, J. H., *et al.* 1978, *Ap. J.*, **220**, 25.
Fazio, G. G., McBreen, B., Stier, M. T., and Wright, E. L. 1980, *Ap. J. (Letters)*, **237**, L39.
Forrest, W. J., McCarthy, J. F., and Houck, J. R. 1979, *Ap. J.*, **233**, 611.
Gilman, R. C. 1972, *Ap. J.*, **178**, 423.
Goldreich, P., and Scoville, N. 1976, *Ap. J.*, **205**, 144.
Herbig, G. H., and Zappala, R. R. 1970, *Ap. J. (Letters)*, **162**, L15.
Hildebrand, R. H. 1983, *Quart. J. R.A.S.*, **24**, 267.
Huggins, P. J., and Glassgold, A. E. 1982*a*, *Ap. J.*, **252**, 201.
———. 1982*b*, *A.J.*, **87**, 1828.
Hyland, A. R., Becklin, E. E., Frogel, J. A., and Neugebauer, G. 1972, *Astr. Ap.*, **16**, 204.
Jameson, R. F., Longmore, A. J., McLinn, J. A., and Woolf, N. J. 1974, *Ap. J.*, **190**, 353.
Jewell, P. R., Webber, J. C., and Snyder, L. E. 1980, *Ap. J. (Letters)*, **242**, L29.
Johansson, L. E. B., *et al.* 1984, *Astr. Ap.*, **130**, 227.
Jones, B., Merrill, K. M., Puetter, R. C., and Willner, S. P. 1978, *A.J.*, **83**, 1437.
Jones, T. W., and Merrill, K. M. 1976, *Ap. J.*, **209**, 509.
Joyce, R. R., Capps, R. W., Gillett, F. C., Grasdalen, G., Kleinmann, S. G., and Sargent, D. G. 1977, *Ap. J. (Letters)*, **213**, L125.
Jura, M. 1983*a*, *Ap. J.*, **267**, 647.
———. 1983*b*, *Ap. J.*, **275**, 683.
Kleinmann, S. G., Sargent, D. G., Moseley, H., Harper, D. A., Loewenstein, R. F., Telesco, C. M., and Thronson, H. A., Jr. 1978, *Astr. Ap.*, **65**, 139.
Knapp, G. R., Phillips, T. G., Leighton, R. B., Lo, K. Y., Wannier, P. G., and Wootten, H. A. 1982, *Ap. J.*, **252**, 616.
Koepf, G. A., Buhl, D., Chin, G., Peck, D. D., Fetterman, H. R., Clifton, B. J., and Tannenwald, P. E. 1982, *Ap. J.*, **260**, 584.
Kwan, J., and Linke, R. A. 1982, *Ap. J.*, **254**, 587.
Kwok, S. 1980, *Ap. J.*, **236**, 592.
Lebofsky, M. J., Kleinmann, S. G., Rieke, G. H., and Low, F. J. 1976, *Ap. J. (Letters)*, **206**, L157.
Lebofsky, M. J., and Rieke, G. H. 1977, *A.J.*, **82**, 646.
Leung, C. M. 1975, *Ap. J.*, **199**, 340.
———. 1976, *J. Quant. Spectrosc. Rad. Transf.*, **16**, 559.
Lo, K. Y., and Bechis, K. 1976, *Ap. J. (Letters)*, **205**, L21.
Low, F. J., Rieke, G. H., and Armstrong, K. R. 1973, *Ap. J. (Letters)*, **183**, L105.
Mathis, J. S., Rumpl, W., and Nordsieck, K. H. 1977, *Ap. J.*, **217**, 425.
Mauron, N., Fort, B., Querci, F., Dreux, M., Fauconnier, T., and Lamy, P. 1984, *Astr. Ap.*, **130**, 341.
McCarthy, J. F., Forrest, J., and Houck, J. R. 1978, *Ap. J.*, **224**, 109.
Merrill, K. M., and Ridgway, S. T. 1979, *Ann. Rev. Astr. Ap.*, **17**, 9.
Merrill, K. M., and Stein, W. A. 1976*a*, *Pub. A.S.P.*, **88**, 285.
———. 1976*b*, *Pub. A.S.P.*, **88**, 294.
———. 1976*c*, *Pub. A.S.P.*, **88**, 874.
Mezger, P. E., Mathis, J. S., and Panagia, N. 1982, *Astr. Ap.*, **105**, 372.
Mitchell, R. M., and Robinson, G. 1980, *M.N.R.A.S.*, **190**, 669.
Morris, M. 1980, *Ap. J.*, **236**, 823.
Morris, M., and Jura, M. 1983*a*, *Ap. J.*, **264**, 546.
———. 1983*b*, *Ap. J.*, **267**, 179.
Moseley, H. 1980, *Ap. J.*, **238**, 892.
Mufson, S. L., Lyon, J., and Marionni, P. A. 1975, *Ap. J. (Letters)*, **201**, L85.
Newell, R. T., and Hjellming, R. M. 1982, *Ap. J., (Letters)*, **263**, L85.
Ney, E. P., Merrill, K. M., Becklin, E. E., Neugebauer, G., and Wynn-Williams, C. G. 1975, *Ap. J. (Letters)*, **198**, L129.
Olofsson, H., Johansson, L., Nguyen-Quang-Rieu, Sopka, R. J., and Zuckerman, B. 1982, *Bull. AAS*, **14**, 894.
Phillips, J. P., White, G. J., Ade, P. A. R., Cunningham, C. T., Richardson, K. J., Robson, E. I., and Watt, G. D. 1982, *Astr. Ap.*, **116**, 130.
Poynter, R. C., and Pickett, H. M. 1981, JPL Pub. 80-32, Rev. 1.
Price, S. G., and Walker, R. G. 1976, AFGL Infrared Sky Survey, Environmental Research Papers, No. 576.
Rowan-Robinson, M. 1980, *Ap. J. Suppl.*, **44**, 403.
Rowan-Robinson, M., and Harris, S. 1983*a*, *M.N.R.A.S.*, **202**, 767.
———. 1983*b*, *M.N.R.A.S.*, **202**, 797.
Shivanandan, K., McNutt, D. P., Daehler, M., and Moore, W. J., 1977, *Nature*, **265**, 515.
Sibille, F., Lunel, M., and Bergeat, J. 1976, *Astr. Ap.*, **47**, 161.
Simon, T., Morrison, D., and Cruikshank, T. 1972, *Pub. A.S.P.*, **84**, 643.
Strecker, D. W., and Ney, E. P. 1974, *A.J.*, **79**, 1410.
Sutton, E. C., Betz, A. L., Storey, J. W. V., and Spears, D. L. 1979, *Ap. J. (Letters)*, **230**, L105.
Telesco, C. M., and Harper, D. A. 1977, *Ap. J.*, **211**, 475.
Werner, M. W., Beckwith, S. E., Gatley, I., Sellgren, K., Berriman, G., and Whiting, D. L. 1980, *Ap. J.*, **239**, 540.
Westbrook, W. E., Becklin, E. E., Merrill, K. M., Neugebauer, G., Schmidt, M., Willner, S. P., and Wynn-Williams, C. G. 1975, *Ap. J.*, **202**, 407.
Whitcomb, S. E., Gatley, I., Hildebrand, R. H., Keene, J., Sellgren, K., and Werner, M. W. 1981, *Ap. J.*, **246**, 416.
Whitcomb, S. E., Hildebrand, R. H., and Keene, J. 1980, *Pub. A.S.P.*, **92**, 863.
Whitcomb, S. E., and Keene, J. 1980, *Appl. Optics*, **19**, 197.
Willner, S. P., Becklin, E. E., and Visvanathan, N. 1972, *Ap. J.*, **175**, 699.
Wright, E. L. 1976, *Ap. J.*, **210**, 250.
Wright, E. L., and Odenwald, S. 1980, *Bull. AAS*, **12**, 456.
Wynn-Williams, C., Becklin, E. E., and Neugebauer, G. 1974, *Ap. J.*, **187**, 473.
Zappala, R. R., Becklin, E. E., Mathews, K., and Neugebauer, G. 1974, *Ap. J.*, **192**, 109.
Zuckerman, B. 1978, *IAU Symposium No. 76, Planetary Nebulae*, ed. Y. Terzian (Dordrecht: Riedel), p. 185.
———. 1980, *Ann. Rev. Astr. Ap.*, **18**, 263.
———. 1981, *A.J.*, **86**, 84.
Zuckerman, B., Gilra, D. P., Turner, B. T., Morris, M., and Palmer, P. 1976, *Ap. J. (Letters)*, **205**, L15.
Zuckerman, B., Palmer, P., Gilra, D. P., Turner, B. T., and Morris, M. 1978, *Ap. J. (Letters)*, **220**, L53.

IAN GATLEY: UKIRT, 900 Lelani Street, Hilo, HI 96720

ROGER H. HILDEBRAND: Enrico Fermi Institute, University of Chicago, 5640 Ellis Avenue, Chicago, IL 60637

DANIEL T. JAFFE: Space Science Laboratory, University of California, Berkeley, CA 94720

MICHAEL A. JURA and BEN ZUCKERMAN: Department of Astronomy, University of California, Los Angeles, CA 90024

THOMAS P. L. ROELLING and MICHAEL W. WERNER: NASA/Ames Research Center, MS 245-6, Moffett Field, CA 94035

ROBERT J. SOPKA: Physics Department, Catonsville Community College, 800 S. Rolling Road, Catonsville, MD 21228